Available online at www.sciencedirect.com
ScienceDirect
Ceramics International 37 (2011) 2821–2828
CERAMICS INTERNATIONAL
www.elsevier.com/locate/ceramint

Effects of the structural layer in MEMS substrates on mechanical and electrical properties of $Pb(Zr_{0.52}Ti_{0.48})O_3$ films

Dan Liu [a], Bo Zhou [a], Sang H. Yoon [a], Howard C. Wikle III [a], Yaqi Wang [b], Minseo Park [b], Barton C. Prorok [a], Dong-Joo Kim [a,*]

[a] *Materials Research and Education Center, Auburn University, AL 36849, USA*
[b] *Department of Physics, Auburn University, 206 Allison Lab, Auburn, AL 36849, USA*

Received 23 February 2011; received in revised form 22 April 2011; accepted 27 April 2011
Available online 14 May 2011

Abstract

In this paper, we describe the effects of the structural layer in substrates on the mechanical and electrical properties of $Pb(Zr_{0.52}Ti_{0.48})O_3$ (PZT) films for MEMS applications. The PZT films were deposited by a sol–gel method on platinized silicon substrates where silicon nitride and silicon oxide were used as a structural layer. The mechanical properties of PZT films were characterized by nanoindentation. The ferroelectric and dielectric properties as a function of film thickness and layer material were investigated. Residual stresses in PZT films were also characterized by Raman spectroscopy. The measured mechanical properties of PZT films on two types of substrate indicate that the structural layer has significant influence on the obtained indentation moduli of PZT films. The PZT on SiN_x-based substrates, i.e., PZT//SiN_x/Si multilayer structure presented higher measured values than those of PZT on SiO_2-based substrate, i.e., PZT//SiO_2/Si multilayer structure throughout the whole indentation depth. The substrate effect on film hardness, however, was negligible since hardness value of around 8.8 GPa was measured for both PZT on SiN_x and SiO_2-based substrates. Significant influences of the film thickness and substrate type on the electrical properties were not observed for the investigated thickness range of the PZT films.

Keywords: C. Mechanical properties; C. Electrical properties; D. PZT; E. Substrates

1. Introduction

PZT films are widely used in microelectromechanical systems (MEMS) due to their large piezoelectric coefficients, dielectric constants, and excellent electromechanical properties [1,2]. To optimize PZT films and design the MEMS devices for the applications, it is imperative to perform a thorough study of their properties. The piezoelectric properties of PZT films are influenced by the material's mechanical coefficients due to the plane stress condition of the film on a thick substrate. In recent years, much attention has been given to the measurement of the mechanical properties of PZT films. Among the methods used to characterize the mechanical properties of films such as impulse acoustic method, micro-beam cantilever deflection technique, atomic force microscopy, etc., the nanoindentation technique can exhibit high sensitivity and does not require the removal of the film from its substrate [3,4]. Several reports on the utilization of nanoindentation for characterization of PZT films have been published. Fang et al. [5] investigated the influence of annealing temperature on the nanomechanical properties of PZT films. Wang et al. [6] reported the crystallographic orientation dependence of the mechanical properties. Delobelle et al. [3,7] measured the mechanical properties of PZT films deposited on various electrode materials. Xu et al. [4] and Chima-Okereke et al. [8] also investigated the mechanical properties of PZT films as a function of indentation depth. The results showed that the experimental data were relatively constant because of negligible substrate effects at small indentation depths. To the best of our knowledge, however, there is no report on the effects of a substrate structural layer on the mechanical and electrical properties of PZT films. In piezoelectric MEMS design, a structural layer of silicon nitride or silicon oxide is commonly used. Therefore, accurate knowledge of its influence

* Corresponding author. Tel.: +1 334 844 4864; fax: +1 334 844 3400.
E-mail address: dkim@eng.auburn.edu (D.-J. Kim).

0272-8842/$36.00
doi:10.1016/j.ceramint.2011.04.125

on the PZT films can be essential to achieve optimum geometric and functional design.

In this study, two sets of PZT films grown on either silicon nitride-based or silicon oxide-based substrates were prepared by a sol–gel method. Different thicknesses of PZT films were evaluated. The mechanical properties of the films were characterized through nanoindentation testing and the electrical properties were analyzed to correlate the film's electromechanical properties to the type of the structural layer and the effect of the film thickness.

2. Experiment and principle

2.1. Film fabrication

Commercially available PZT sol–gel solutions (110/52/48) (Inostek Inc., South Korea) were spin-coated on 10 mm × 10 mm Pt(1 1 1)/Ta/SiO_2/Si or Pt(1 1 1)/Ta/SiN_x/Si substrates at 4000 rpm for 20 s followed by drying at 150 °C for 2 min and pyrolysis at 300 °C for 10 min. Such coating and pyrolysis treatments were repeated for 6, 9, and 12 times to obtain a set of films whose thicknesses are 580, 830, and 1130 nm, respectively. A pre-annealing process was carried out at 650 °C for 15 min every three times, and a final annealing was conducted at 650 °C for 1 h after obtaining the desired film thickness to ensure the formation of perovskite phase. Fig. 1 shows a schematic diagram for the preparation of PZT films.

2.2. Nanoindentation measurements

Nanoindentation tests were performed using an MTS NanoIndenter XP system (MTS Nano Instruments, Knoxville, TN) with the combination of both a continuous stiffness method (CSM) and static method. The CSM has the target harmonic displacement amplitude of 2 nm and a minimum thermal drift rate of 0.05 nm/s. From the method developed by Oliver and Pharr [9], the hardness and modulus can be determined by indentation load–displacement data according to the following equations [10]:

$$H = \frac{P_{\max}}{A} \tag{1}$$

$$E = (1 - v^2)\left[\frac{2}{\sqrt{\pi}}\beta\frac{\sqrt{A}}{S} - \frac{1 - v_i^2}{E_i}\right] \tag{2}$$

where $P_{\max}$ is the peak indentation load, A is the projected area of contact under load, β is a constant that depends on the geometry of the indenter tip (a Berkovich tip was used in this study, $\beta = 1.034$.), S is the experimentally measured contact stiffness, v is the Poisson's ratio for the test material, and E_i and v_i are the elastic modulus and Poisson's ratio of the indenter, respectively. For diamond, the elastic constants E_i and v_i are equal to 1141 GPa and 0.07 [7,11].

When the mechanical properties of PZT films were measured by a nanoindentation method, the following statements were commonly advised:

(1) The indentation depths were limited to less than a tenth of the film thickness (Fig. 2a). (Here, a PZT sample with 12

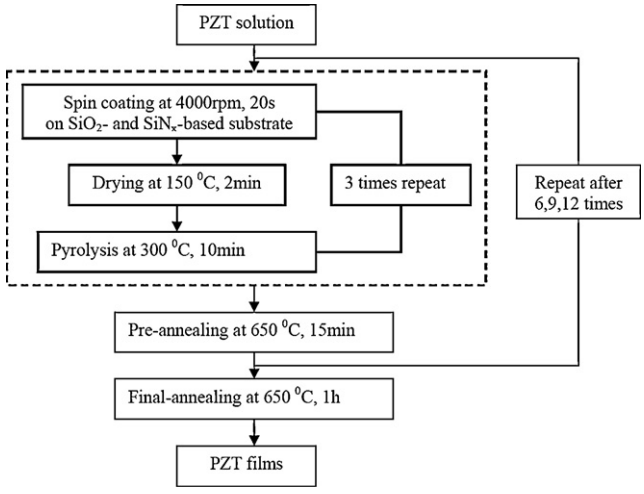

Fig. 1. Schematic diagram for the preparation of PZT films.

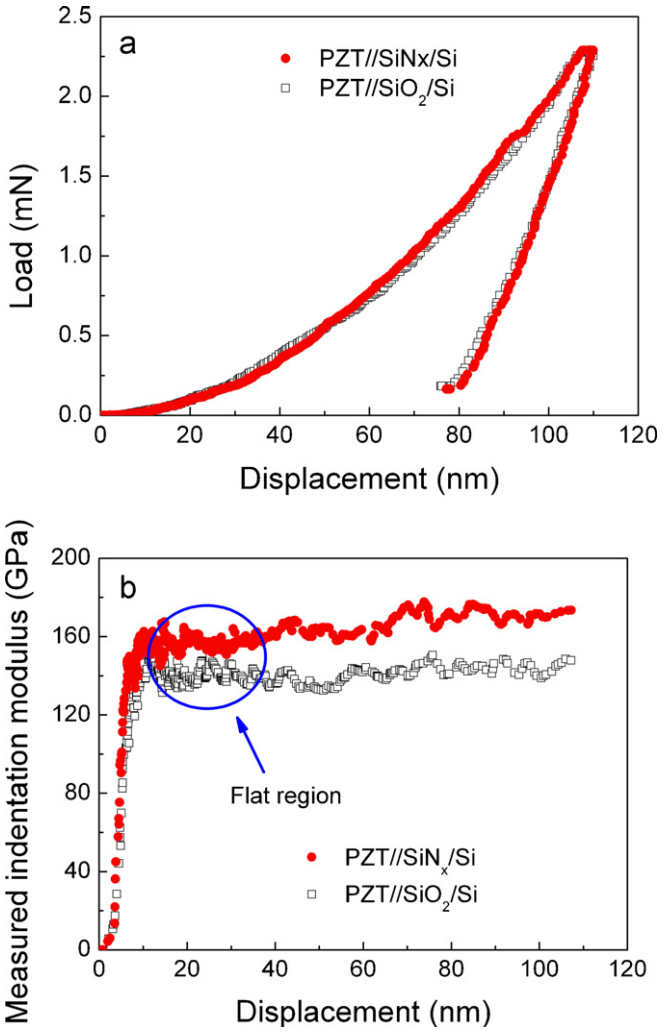

Fig. 2. (a) Load–displacement and (b) measured indentation modulus–displacement curves of 1130 nm PZT films.

times deposition was taken as an example) According to the one-tenth ''rule of thumb'', the measured mechanical property can be very close to true value of a film if the film is ten times thicker than the indentation depth [6,12,13]. Microcracks and pile-ups do not occur in PZT films because the applied loads were very low at small indentation depths [3]. As shown in the curves of load–displacement of Fig. 2a, no discontinuity is observed which indicates that microcracks do not occur in the indentation process [14,15].

(2) The indentation modulus is obtained from the flat regions (Fig. 2b) where the values are relatively constant and can be considered as a representative of the film modulus [16].

2.3. Electrical and spectroscopic characterization

For electrical measurement, platinum top electrodes were deposited by dc magnetron sputtering at room temperature on PZT films through a shadow mask. Typical thickness of Pt top electrodes was 120 nm. A TF-2000 ferro/piezoelectric tester (aixACCT Systems GmbH, Germany) was used for the measurement of field-induced polarization. Dielectric properties were measured using a HP 4192A impedance analyzer. An oscillation signal typically10 kHz in frequency and 0.1 Vrms in amplitude was used. Residual stress in PZT films was characterized by Raman spectroscopy that was performed using the 441.6 nm line from a He–Cd laser (80 mW). Raman spectra were collected using a spectrometer (JY-550) equipped with two 3-in. holographic gratings (2400 lines/mm, 3600 lines/mm), and a thermoelectrically cooled charge coupled device (CCD) detector (2048 × 512 pixels).

3. Results and discussion

3.1. Mechanical properties

Three different thicknesses of PZT films and two types of structural layers were prepared and characterized. For each sample, 20 CSM tests were conducted at the same indentation depth. Fig. 3 shows the evolution of the measured indentation modulus of PZT films grown on different substrates with varying film thickness. Since the preferred orientation and the microstructure of the PZT films can contribute to different mechanical properties [3,6,7,17], all samples were characterized using scanning electron microscopy (SEM) and X-ray diffraction (XRD). Fig. 4 shows the XRD patterns of the PZT films. All samples show strong (1 1 1) orientation because lattice matching between PZT and (1 1 1) platinum bottom electrode seems dominant in these films irrespective of the types of structural layer [18]. Fig. 5 shows the surface morphologies of the crystallized PZT films. Almost identical surface topographies are observed in these films and the grain sizes are in the range of 60–280 nm. The above results indicate that the influences of orientation and microstructure on the measured indentation moduli of PZT films can be neglected. When comparing PZT films on different structural layers, the PZT films on SiN_x-based substrates, i.e., PZT//SiN_x/Si multilayer structure show higher indentation moduli than those on SiO_2-based substrates, i.e., PZT//SiO_2/Si multilayer structure even at penetration depths less than 10% of the film thickness as shown in Fig. 6a. Different indentation moduli from PZT film structures having similar microstructure and orientation indicate that the commonly used one-tenth rule may not be adequate to determine the true film modulus because of convolution of PZT films and substrates. Our previous work [19] proposed a two-layer model that described how to extract the actual Young's modulus of a film on a substrate by investigating 25 different combinations of 5 films on 5 substrates. The previous work showed that the value in the flat region used to determine the true modulus can be influenced by both the film and substrate. The measured indentation moduli of the films could be influenced by the substrate even at indentation depths less than 2% of the film thickness. Therefore, the flat region observed in Fig. 2b may still be influenced by the substrate. The indentation moduli of two different structural layers prior to PZT film deposition are

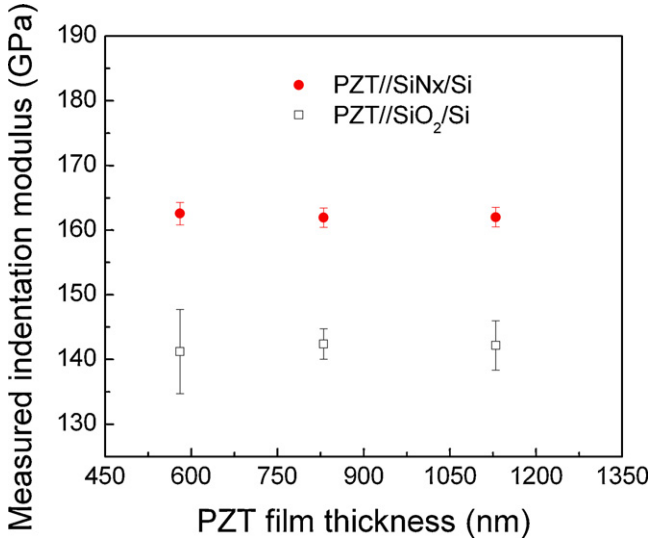

Fig. 3. Measured indentation modulus as a function of the thickness of PZT films on SiO_2/Si and SiN_x/Si substrates.

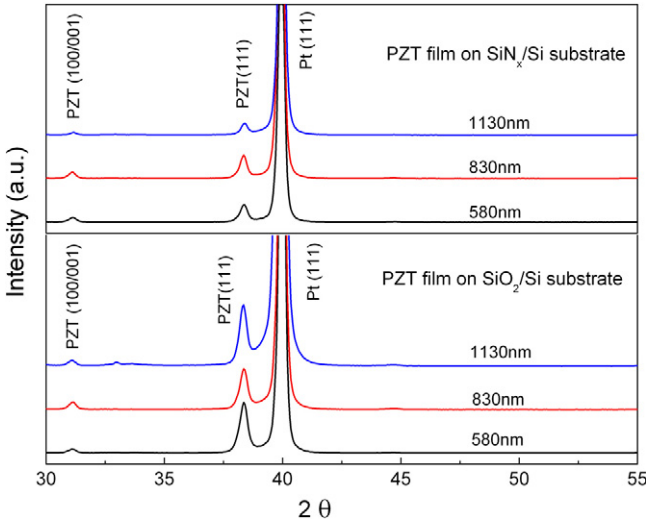

Fig. 4. XRD patterns of PZT films with different substrates and thicknesses.

shown in Fig. 6b. The plot clearly shows that the measured indentation moduli of PZT film multilayer structures were strongly influenced by the structure layer, i.e., substrate structure.

The nanoindentation measurement up to an indentation depth of 2200 nm was conducted on 1130 nm thick PZT films to investigate the evolution of the modulus as a function of indentation depth. As shown in Fig. 6a, the measured indentation modulus of the PZT//SiN_x/Si multilayer structure tends to increase as a function of indentation depth until around 300 nm. Then the value decreases until the indentation depth of 1122 nm where the fracture point occurs. Such interface failure between PZT and substrate was also confirmed in a load–displacement curve (Fig. 7a) similar to the results found in the literature [14,15]. The discontinuity in the curve shows that the delamination and cracking occurred at the PZT/Pt interface as can be seen in Fig. 7b. The results for the PZT//SiO_2/Si multilayer structure also showed a very similar trend, but different maximum modulus value and fracture point position were observed. The maximum modulus value of the PZT//SiO_2/Si multilayer structure was around 200 nm, which was smaller than that of the PZT//SiN_x/Si multilayer structure.

During the early stage of nanoindentation, the measured indentation modulus values increase with increasing depth and the curve becomes very steep. The data collected in this stage, according to the work by Pharr et al. [20], are under the influences of displacement oscillation and are significantly underestimated due to the loss of contact with the indenter. Therefore, the increasing modulus values should not be attributed to the influence of the substrates. As the indenter goes deeper into the film, the effects caused by indenter oscillation become negligible and the substrate effect dominates the indentation process. The measured indentation modulus of the PZT//SiO_2/Si multilayer structure soon

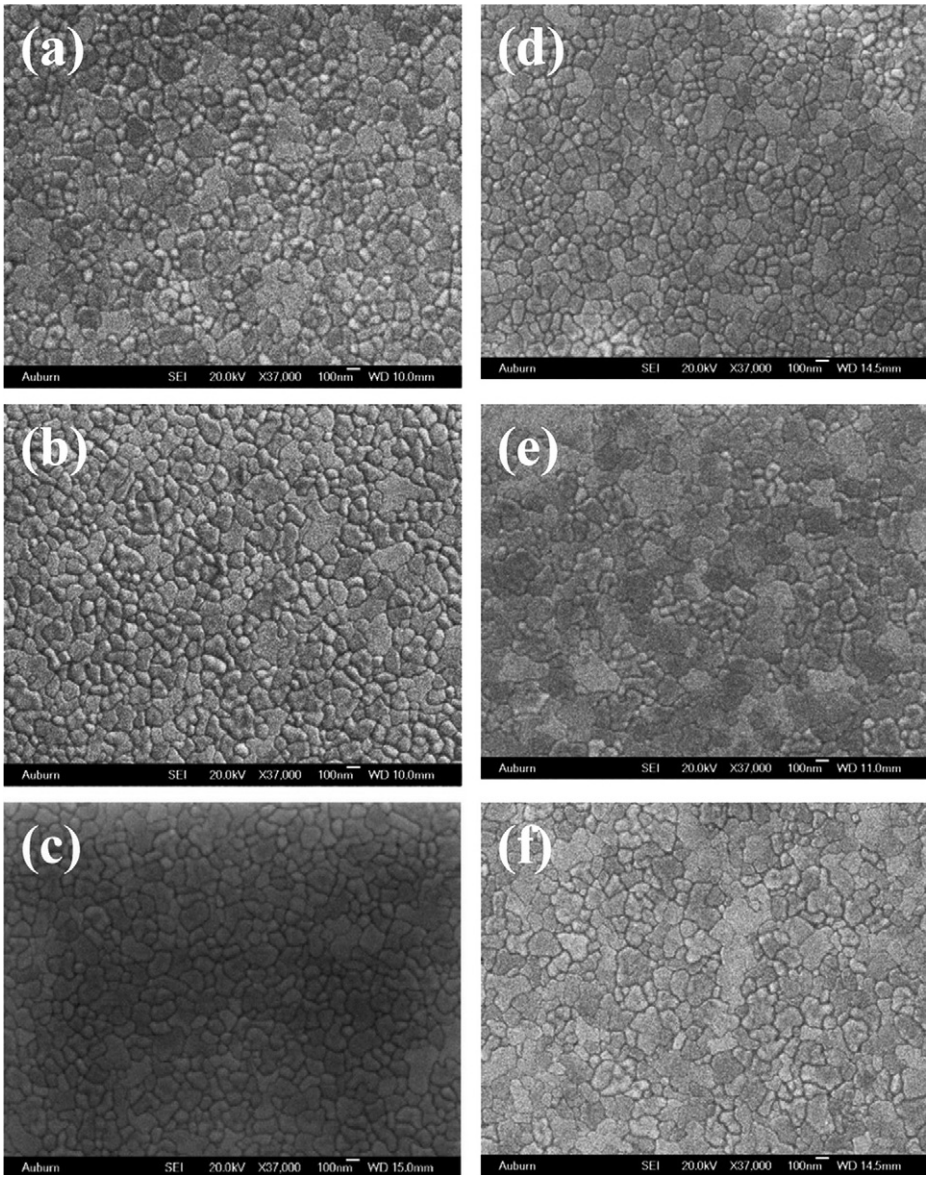

Fig. 5. SEM images for PZT films on SiO_2/Si (left) and SiN_x/Si (right) substrates with different thicknesses: (a) and (d) 580 nm; (b) and (e)830 nm; and (c) and (f)1130 nm (all have 60–220 nm grain size).

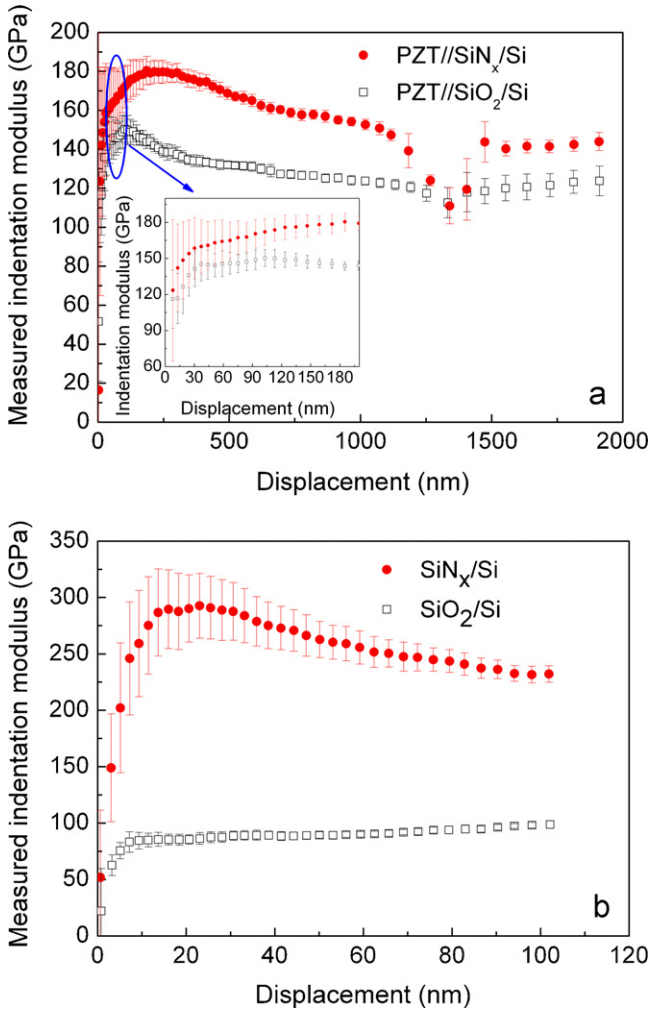

Fig. 6. Measured indentation modulus as a function of displacement (a) with 2200 nm depth limit for PZT//SiO_2/Si and PZT//SiN_x/Si multilayer structures (b) for SiO_2/Si and SiN_x/Si structures.

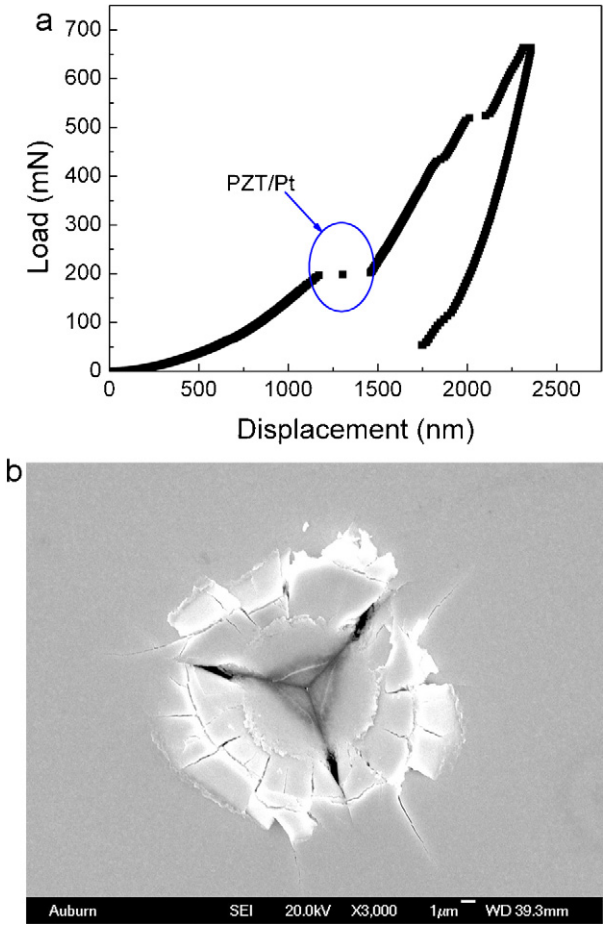

Fig. 7. (a) Load–displacement curve indicating fracture point and (b) SEM image showing delamination and cracking around indentation in case of PZT//SiN_x/Si multilayer structure with 2200 nm depth limit.

decreases due to the influence of the softer SiO_2 substrate while the measured indentation modulus of the PZT//SiO_2/Si multilayer structure continues to increase. After reaching the maximum value, the measured moduli and the modulus difference between two cases becomes smaller because the Si layer is dominating the measurements as the indenter gets closer to Si. It should be pointed out that, in a multilayer structure, the substrate effect is attributed to the combined effect of different layers during the nanoindentation measurement, and therefore the measured indentation modulus values of the PZT//SiN_x/Si structure are always larger than those of the PZT//SiO_2/Si structure even as the indenter penetrates into the Si substrate. For the PZT//SiO_2/Si structure, the facture point was observed at the indentation depth of 1255 nm which is larger than that of the PZT//SiN_x/Si structure, and the reason is probably due to the softer SiO_2 layer being able to absorb more applied strain [21].

The evolution of the hardness as a function of indentation depth is given in Fig. 8. Below indentation depth of approximately 400 nm, the measured hardness of the PZT films on the two types of substrates exhibit similar values of around 8.8 GPa. Deeper indentation depth induces delamination and buckling in PZT structures, but the interfacial cracks do not propagate extensively [15]. The PZT//SiN_x/Si structure exhibited a slightly smaller hardness than PZT//SiO_2/Si structure after 400 nm indentation depth. It is likely that the

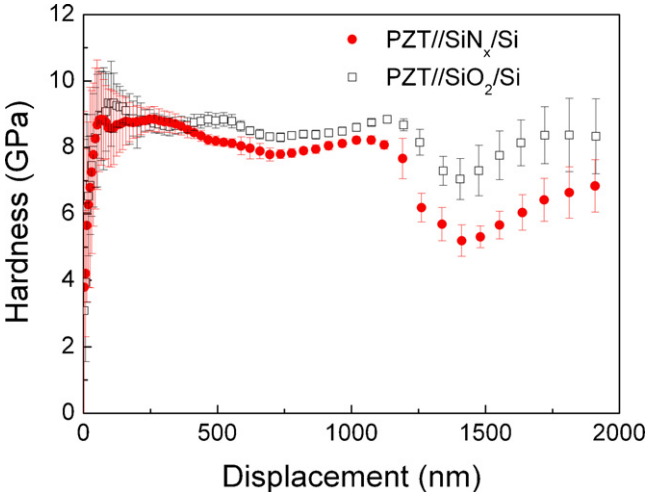

Fig. 8. Hardness as a function of displacement with 2200 nm depth limit for PZT//SiO_2/Si and PZT//SiN_x/Si multilayer structures.

SiN_x layer absorbs only a small amount of the applied strain compared to SiO_2 layer as mentioned above which results in a severe fracture and a larger contact area. According to Eq. (1), the smaller quantity of measured hardness with the PZT//SiN_x/Si structures was expected; however, the difference was very small due to the lack of extensive propagation of the interfacial cracks. When the indentation depth is above 1100 nm, a serious delamination occurs in both structures and results in a larger difference on the measured hardness.

One may argue that the difference in the measured hardness could also be caused by the different substrates. For the measurement of elastic modulus of PZT film, the result will be greatly affected by the substrate even if the indentation depth is very small because the elastic deformation is not confined to the film itself; rather, it is a long-range effect that extends into the substrate [22]. However, for the measurement of hardness of PZT film, the plastic deformation will be confined within the film as the hardness of the substrate is greater than the film in both cases [23–30] (Table 1) and the measured hardness should only represent the true film hardness. This explains why the measured hardness of PZT films on two different substrates show similar value before delamination starts.

3.2. Electrical properties

The remanent polarization and the dielectric constants of the PZT films were characterized as shown in Fig. 9. Both properties were not significantly influenced by the types of structural layer and the observed range of PZT film thickness. It is commonly reported that the remanent polarization and the dielectric constants increase as film thickness increases due to smaller residual stress and/or bigger grain size [31–35]. There exists a critical thickness where this scaling effect becomes negligible, typically in the range of 0.3–0.6 μm, depending on the fabrication conditions. No significant change of the polarization and dielectric constant can be due to thicker films (0.58–1.13 μm) that exceed the critical thickness. The PZT films on different structural layers also showed similar electrical properties. The results can be attributed to similar crystallographic properties such as orientation and microstructure and/or comparable residual stress conditions for the PZT films grown on both structural layers as observed by the XRD and SEM results. Although the structural layer may affect the stress conditions [36], comparable residual stress values from PZT films on both structural layers were estimated that were due to the constraint of the PZT film by the much thicker Si substrate.

Table 1
Description of PZT film structure.

Layer material	Thickness (nm)	Modulus (GPa)	Hardness (GPa)
PZT	580, 830, 1130	125–190 [3,6,7]	5.1–8.6 [3,7,25]
Pt(1 1 1)	120	170 [23]	9.0 [25]
SiO_2	500	70 [26]	14.4–18.0 [24]
SiN_x	500	220 [27]	21.0 [27]
Ta	10	178 [28]	11.6 [28–30]

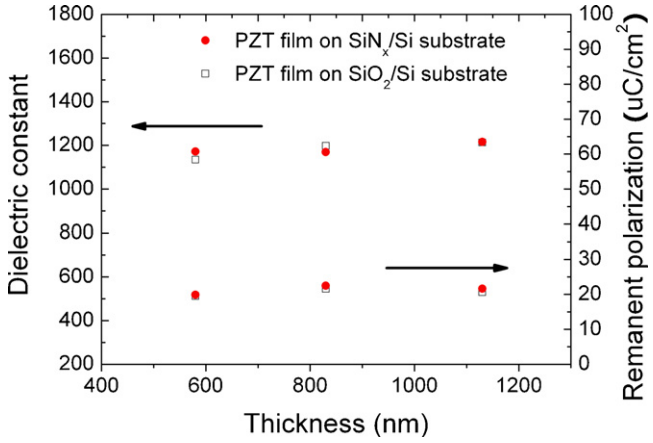

Fig. 9. The electrical properties as a function of the thickness of PZT films on SiO_2/Si and SiN_x/Si substrates.

To confirm the conjecture, Raman scattering was conducted to investigate the residual stress conditions in all PZT films. For PZT, the Raman spectra in the tetragonal phase have the following modes [37]: $A_1(TO_i)$,$A_1(LO_i)$, $E(TO_i)$,$E(LO_i)$ (i = 1,2,3) and some mixed modes such as $B_1 + E$ and others. To avoid the effect of Rayleigh scattering which is strong in the low-frequency region [38,39], the $A_1(TO_3)$ mode was chosen for calculating the residual stress. From the Lydane–Sach–Teller (LST) relation, the dielectric constant is proportional to the square of the phonon frequency of the $A_1(TO_3)$ mode, therefore, the following equation can be used to calculate the residual stress in PZT films [40,41]:

$$\omega^2 = \omega_0^2\left(1 - \frac{\sigma}{\sigma_1}\right) \tag{3}$$

where σ_1 is the stress under which the phonon frequency becomes zero and ω_0 is the phonon frequency under zero stress. By using the bulk-PZT sample and fitting the obtained data, $\sigma_1 = -640.7$ MPa and $\omega_0 = 528.8$ cm^{-1} for the $A_1(TO_3)$ mode were calculated [41]. The Raman spectra for PZT films are shown in Fig. 10 and summarized in Table 2 after background correction and Lorentzian fitting. It is well known that the phonon frequency shift is related to residual stress, crystal size, temperature and crystal structure [38]. The last two factors can be excluded at first because the Raman scattering was conducted at room temperature and the crystal structures were identical as checked by XRD. For the grain size, all samples show similar range and it was found that the wave number shift of $A_1(TO_3)$ mode is less than 2 cm^{-1} for grain size larger than 17 nm [41]. Therefore, the frequency shift in our case should be caused by the residual stress in the PZT films. The obtained results show stress values of PZT films with different thicknesses are very close and in the range of 88–101 MPa. It should be noted that the 10 MPa difference of stresses of PZT film on different substrates will not result in significant change of electric properties since previously reported work [33] showed a 30 MPa change in applied stress caused only a 2% change in electric properties.

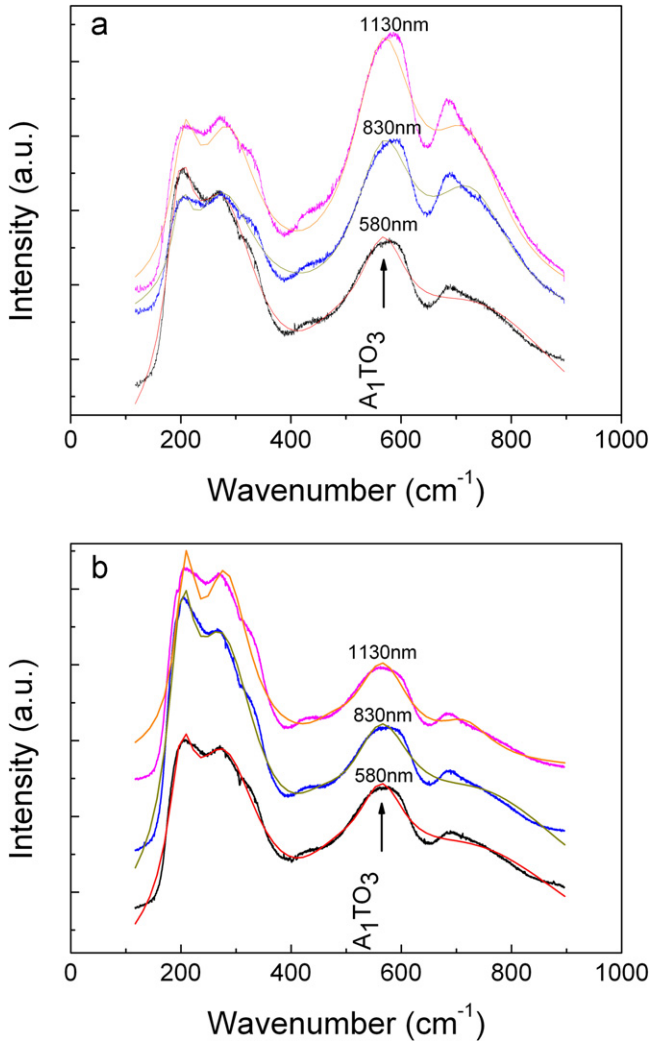

Fig. 10. Raman spectra of PZT films on (a) SiO_2/Si and (b) SiN_x/Si substrate.

Table 2
The extracted residual stresses in the PZT films based on $A_1(TO_3)$ mode after background subtraction and Lorentz fitting.

Thickness (nm)	PZT on SiO_2-based substrate		PZT on SiN_x-based substrate	
	Freq. (cm^{-1})	Stress (MPa)	Freq. (cm^{-1})	Stress (MPa)
580 (6t)	568	98	564	88
830 (9t)	569	101	564	88
1130 (12t)	568	98	566	93

4. Conclusions

The use of a structural layer such as silicon dioxide or silicon nitride resulted in a difference in the indentation moduli of the PZT films because of the combined response of PZT films and substrates in nanoindentation measurement. The measured indentation moduli of the PZT films on SiN_x-based substrates, i.e., PZT//SiN_x/Si multilayer structures show higher values than those of the PZT films on SiO_2-based substrates, i.e., PZT//SiO_2/Si multilayer structures for indentation depths up to 2200 nm. The results demonstrate how substrate structures and properties influence the measured indentation moduli and how such effects might not be avoidable without a complete analytical solution in order to extract the true values from the flat regions in the modulus–displacement curves. However, the structural layer does not show significant influence on the hardness of the PZT films. The measured values were about 8.8 GPa because the plastic deformation was entirely contained in the PZT film due to the harder substrate material. Irrespective of the types of structural layer, similar electrical properties were observed in the characterized PZT thickness range. Similar microstructure and texture of the PZT films in addition to residual stress conditions determined by Raman characterization appear to be the reasons for similar electrical properties.

Acknowledgements

This work was supported by a research grant from the National Science Foundation (NSF-DMR-0605270), and Auburn University Detection and Food Safety Center funded by USDA.

References

[1] B. Jaffe, W.R. Cook, H. Jaffe, Piezoelectric Ceramics, Academic Press, London, 1971.
[2] D. Shen, J.-H. Park, J.H. Noh, S.-Y. Choe, S.-H. Kim, H.C. Wikle III, D.-J. Kim, Micromachined PZT Cantilever based on SOI structure for Low Frequency Vibration Energy Harvesting, Sens. Actuators A 154 (2009) 103–108.
[3] P. Delobelle, E. Fribourg-Blanc, D. Remiens, Mechanical properties determined by nanoindentation tests of [Pb(Zr,Ti)O_3] and [Pb($Mg_{1/3}Nb_{2/3}$)1 − $x$$Ti_xO_3$] sputtered thin films, Thin Solid Films 515 (2006) 1385–1393.
[4] X.H. Xu, P. Gu, R. Jiang, G. Zhao, L. Wen, J.R. Chu, 1st IEEE International Conference on Nano/Micro Engineered and Molecular Systems, Zhuhai, China, (2006), pp. 56–60.
[5] T.-H. Fang, S.-R. Jian, D.-S. Chuu, Nanomechanical properties of lead zirconate titanate thin films by nanoindentation, J. Phys.: Condens. Matter 15 (2003) 5253–5259.
[6] Q.-M. Wang, Y. Ding, Q. Chen, M. Zhao, J. Cheng, Crystalline orientation dependence of nanomechanical properties of Pb($Zr_{0.52}$ $Ti_{0.48}$)O_3 thin films, Appl. Phys. Lett. 86 (2005) 162903.
[7] P. Delobelle, G.S. Wang, E. Fribourg-Blanc, D. Remiens, Indentation modulus and hardness of Pb(Zr, Ti)O_3 sol–gel films deposited on Pt and $LaNiO_3$ electrodes An estimation of the C_{ij}^D compliances, J. Eur. Ceram. Soc. 27 (2007) 223–230.
[8] C. Chima-Okereke, A.J. Bushby, M.J. Reece, R.W. Whatmore, Q. Zhang, Experimental, analytical, and finite element analyses of nanoindentation of multilayer PZT/Pt/SiO_2 thin film systems on silicon wafers, J. Mater. Res. 21 (2006) 409–419.
[9] W.C. Oliver, G.M. Pharr, Improved technique for determining hardness and elastic modulus using load and displacement sensing indentation experiments, J. Mater. Res. 7 (1992) 1564–1580.
[10] X. Li, B. Bhushan, A review of nanoindentation continuous stiffness measurement technique and its applications, Mater. Charact. 48 (2002) 11–36.
[11] G. Simmons, H. Wang, Single Crystal Elastic Constants and Calculated Aggregate Properties: A Handbook, The M.I.T. Press, 1971.
[12] ASTM Standard Test Method E 384, American Society for Testing and Materials, 1989.
[13] G.N. Peggs, I.C. Leigh, Recommended Procedure for Microindentation Vickers Hardness Test, UK National Physical Laboratory, 1983.

[14] P. Delobelle, G.S. Wang, E. Fribourg-Blanc, D. Remiens, Mechanical properties measured by nano-indentation of Pb(Zr, Ti)0_3 sol–gel films deposited on Pt and LaNi0_3 electrodes, Surf. Coat. Technol. 201 (2006) 3155–3162.

[15] X.J. Zheng, Y.C. Zhou, J.Y. Li, Nano-indentation fracture test of $Pb(Zr_{0.52}Ti_{0.48})O_3$ ferroelectric thin films, Acta Mater. 51 (2003) 3985–3997.

[16] J.L. Hay, G.M. Pharr, Mechanical testing and evaluation, in: H. Kuhn, D. Medlin (Eds.), ASM Handbook, vol. 8, ASM International, 2000, pp. 232–243.

[17] H. Wu, L. Wu, Q. Sun, W. Fei, S. Du, Mechanical properties of sol–gel derived lead zirconate titanate thin films by nanoindentation, Appl. Surf. Sci. 254 (2008) 5492–5496.

[18] J.H. Park, S.H. Yoon, D. Shen, S.Y. Choe, Y.S. Yoon, M. Park, D.J. Kim, Effects of preferred orientation on the piezoelectric properties of Pt/$Pb(Zr_{0.3}Ti_{0.7})O_3$/Pt thin films grown by sol–gel process, J. Mater. Sci.: Mater. Electron. 20 (2009) 366–373.

[19] B. Zhou, B.C. Prorok, A new paradigm in thin film indentation, J. Mater. Res. 25 (2010) 1671–1678.

[20] G.M. Pharr, J.H. Strader, W.C. Oliver, Materials Research Society, Keystone Drive, Warrendale, PA 15086, United States, 506, 2009, 653–666.

[21] D.C. Van Der Laan, J.W. Ekin, C.C. Clickner, T.C. Stauffer, Delamination strength of YBCO coated conductors under transverse tensile stress, Supercond. Sci. Technol. 20 (2007) 765–770.

[22] R. Saha, W.D. Nix, Effects of the substrate on the determination of thin film mechanical properties by nanoindentation, Acta Mater. 50 (2002) 23–38.

[23] IEEE, Micro Electro Mechanical Systems Workshop, February, Napa Valley, CA, (1990), p. 174.

[24] IEEE, Micro Electro Mechanical Systems Workshop, February, San Diego, CA, (1996), p. 97.

[25] D.F. Bahr, J.S. Robach, J.S. Wright, L.F. Francis, W.W. Gerberich, Mechanical deformation of PZT thin films for MEMS applications, Mater. Sci. Eng. A 259 (1999) 126–131.

[26] M.T. Kim, Influence of substrates on the elastic reaction of films for the microindentation tests, Thin Solid Films 283 (1996) 12–16.

[27] J.J. Vlassak, W.D. Nix, A new bulge test technique for the determination of Young's modulus and Poisson's ratio of thin films, J. Mater. Res. 7 (1992) 3242–3249.

[28] M. Zhang, B. Yang, J. Chu, T.G. Nieh, Hardness enhancement in nanocrystalline tantalum thin films, Scripta Mater. 54 (2006) 1227–1230.

[29] Z.Z. Tang, J.H. Hsieh, S.Y. Zhang, C. Li, Y.Q. Fu, Phase transition and microstructure change in Ta–Zr alloy films by co-sputtering, Surf. Coat. Technol. 198 (2005) 110–113.

[30] J.H. Hsieh, C. Li, C.M. Wang, Z.Z. Tang, Boundary-free multi-element barrier films by reactive co-sputtering, Surf. Coat. Technol. 198 (2005) 335–339.

[31] T.A. Berfield, R.J. Ong, D.A. Payne, N.R. Sottos, Residual stress effects on piezoelectric response of sol–gel derived lead zirconate titanate thin films, J. Appl. Phys. 101 (2007).

[32] T. Haccart, E. Cattan, D. Remiens, Dielectric, ferroelectric and piezoelectric properties of sputtered PZT thin films on Si substrates: influence of film thickness and orientation, Semicond. Phys. Quantum Electron. Optoelectron. 5 (2002) 78–88.

[33] R.J. Ong, D.A. Payne, N.R. Sottos, Processing effects for integrated PZT: residual stress, thickness, and dielectric properties, J. Am. Ceram. Soc. 88 (2005) 2839–2847.

[34] Z.Z. Tang, S.J. Liu, R.K. Singh, S. Bandyopadhyay, I. Sus, T. Kotani, M.v. Schilfgaarde, N. Newman, Growth and characterization of epitaxial $Ba(Zn_{1/3}Ta_{2/3})O_3$ (1 0 0) thin films, Acta Mater. 57 (2009) 432–440.

[35] S. Bandyopadhyay, S.J. Liu, Z.Z. Tang, R.K. Singh, N. Newman, Leakage–current characteristics of vanadium- and scandium-doped barium strontium titanate ceramics over a wide range of DC electric fields, Acta Mater. 57 (2009) 4935–4947.

[36] J. Baborowski, Microfabrication of piezoelectric MEMS, J. Electroceram. 12 (2004) 33–51.

[37] J.F. Meng, R.S. Katiyar, G.T. Zou, X.H. Wang, Raman phonon modes and ferroelectric phase transitions in nanocrystalline lead zirconate titanate, Phys. Status Solidi A 164 (1997) 851–862.

[38] T. Ohno, T. Matsuda, K. Ishikawa, H. Suzuki, Thickness dependence of residual stress in alkoxide-derived $Pb(Zr_{0.3}Ti_{0.7})O_3$ thin film by chemical solution deposition, Jpn. J. Appl. Phys. 45 (2006) 7265–7269, Part 1: Regular Papers and Short Notes and Review Papers.

[39] H. Yi, M.G. Kim, J.H. Park, H.M. Jang, Polarized Raman scattering of highly [1 1 1]-oriented Pb(Zr, Ti)O_3 thin films in the rhombohedral-phase field, J. Appl. Phys. 96 (2004) 5110–5116.

[40] J.H. Lee, K.S. Hwang, T.S. Kim, Microstress relaxation effect of $Pb(Zr_{0.52}Ti_{0.48})$ O_3 films with thicknesses for micro/nanopiezoelectric device, Appl. Phys. Lett. 96 (2010) 092904.

[41] W.H. Xu, D. Lu, T.Y. Zhang, Determination of residual stresses in $Pb(Zr_{0.53}Ti_{0.47})O_3$ thin films with Raman spectroscopy, Appl. Phys. Lett. 79 (2001) 4112–14112.